The photon PDF from high-mass Drell-Yan data at the LHC

*V. Bertone**
Department of Physics and Astronomy, VU University, NL-1081 HV Amsterdam,
and Nikhef Theory Group Science Park 105, 1098 XG Amsterdam, The Netherlands

Abstract
I present a determination of the photon PDF from a fit to the recent ATLAS measurements of high-mass Drell-Yan lepton-pair production at $\sqrt{s} = 8$ TeV. This analysis is based on the `xFitter` framework interfaced to the `APFEL` program, that accounts for NLO QED effects, and to the `aMCfast` code to account for the photon-initiated contributions within `MadGraph5_aMC@NLO`. The result is compared with other recent determinations of the photon PDF finding a general good agreement. This writeup is based on the results presented in Ref. [1].

Keywords
Photon PDF, NLO electroweak corrections, Drell-Yan data.

1 Introduction and motivation

In order to achieve accurate predictions for the LHC phenomenology, QCD corrections, where NNLO is becoming the standard, have to be supplemented with electroweak (EW) effects. One of the direct consequences of these corrections is the introduction of the photon PDF.

An number of determinations of the photon PDF based on a variety of different approaches has been achieved in the past [3–8, 19]. The aim of this particular work is to obtain a model-independent determination of the photon PDF exploiting the recent high-mass Drell-Yan measurements at $\sqrt{s} = 8$ TeV from ATLAS [9], that have proven to provide a significant constraint on this distribution.

The constraining power of the Drell-Yan process on the photon PDF can be easily understood in terms of Feynman diagrams. Indeed, in the presence of EW corrections, the partonic channel $\gamma\gamma \to \ell^+\ell^-$ contributes to the leading order (LO) cross section for lepton-pair production in pp scattering. This is

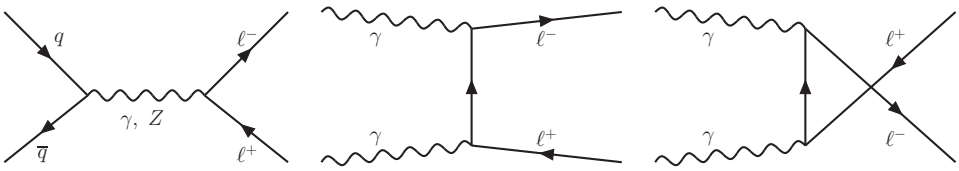

Fig. 1: LO diagrams that contribute to lepton-pair production at hadron colliders.

illustrated in Fig. 1 where the LO diagrams contributing to this process are shown.

The high invariant-mass distribution of the lepton pair is particularly relevant because this observable is such that the $\gamma\gamma$ contribution, despite the relatively small size of the photon PDF, becomes comparable to that induced by the $q\overline{q}$ channel. As an illustration, the LO prediction for the lepton-pair invariant mass distribution in e^+e production at the 13 TeV LHC is shown in Fig. 2 [14]. This plot indicates that the $\gamma\gamma$ channel becomes increasingly important at large values of the invariant mass and eventually dominates the distribution. Based on simple kinematic considerations, one can show that

*On behalf of the `xFitter` developer's team.

https://doi.org/10.23727/CERN-Proceedings-2018-001.91

the high invariant-mass distribution in lepton-pair production probes the photon PDF at relatively large values of Bjorken-x, indicatively $x \gtrsim 0.02$.

This observation constitutes a compelling motivation to exploit the precise experimental data produced by the LHC, such as the recent ATLAS data at 8 TeV published in Ref. [9], to constrain the photon PDF in this region. A crucial aspect of this analysis is the consistent inclusion of the relevant EW corrections. As it was shown in Ref. [15], the Drell-Yan process receives sizeable pure weak corrections that almost balance the corrections induced by the photon-initiated channels. Therefore, the inclusion of the NLO EW corrections to the computation of the Drell-Yan cross sections is extremely important to achieve a reliable determination of the photon PDF. This study was carried out within the open-source `xFitter` framework [10] that provides a unique environment to extract PDFs from experimental data.

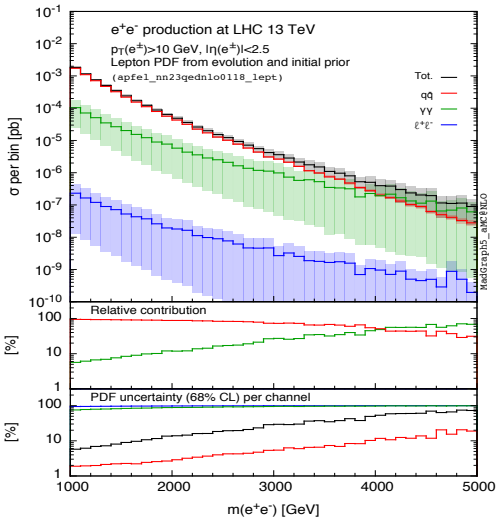

Fig. 2: Predictions at LO for the lepton-pair invariant mass distribution in e^+e production at the LHC at 13 TeV [14].

2 The dataset

As mentioned above, our determination of the photon PDF relies on the recent ATLAS 8 TeV high-mass Drell-Yan data [9]. Measurements are delivered in three different formats:

1. as single-differential cross-section distributions in the lepton-pair invariant mass m_{ll},
2. as double-differential cross-section distributions in m_{ll} and the rapidity of the lepton pair $|y_{ll}|$,
3. and as double-differential cross-section distributions in m_{ll} and the difference in pseudo-rapidity between the two leptons $\Delta\eta_{ll}$.

In our analysis we have chosen to use the second format that counts 48 data points distributed in 5 m_{ll} bins: [116-150], [150-200], [200-300], [300-500], [500-1500] GeV. The first three (last two) m_{ll} bins are divided into 12 (6) bins in $|y_{ll}|$ extending up to 2.4. The relevant analysis cuts on the data are: $m_{ll} \geq 116$ GeV, $|\eta_{ll}| \leq 2.5$, and $p_T^l \geq 40$ GeV (30) GeV for the leading (sub-leading) lepton.

The ATLAS data alone would clearly be insufficient to carry out an analysis aimed at the extraction of a reliable set of PDFs. Therefore, this data is supplemented by the combined inclusive deep-inelastic scattering (DIS) cross-section data from HERA [16], on which we imposed the cut $Q^2 \geq Q^2_{\rm min} = 7.5$ GeV^2. While the ATLAS data is directly sensitive to the photon PDF, the HERA data carries detailed information on the quark and gluon content of the proton. The union of these two datasets allows us to perform a solid determination of a the proton PDFs.

3 Electroweak corrections

A central aspect of this analysis is the inclusion of the EW effects. More in particular, we employed predictions accurate to NNLO in QCD and consistently included NLO EW/QED corrections. In the present analysis, this concerns three main sectors which I discuss in turn: the QED corrections to the evolution of PDFs, the QED corrections to the DIS structure functions, and the full EW corrections to the Drell-Yan cross sections.

3.1 Evolution

The evolution of PDFs is governed by the DGLAP equations. The DGLAP splitting functions are known up to $\mathcal{O}(\alpha_s^3)$, *i.e.* NNLO in QCD, since long [17,18]. The QED corrections are instead much more recent. The $\mathcal{O}(\alpha)$ corrections, where α is the QED coupling, were derived in Ref. [19], while the $\mathcal{O}(\alpha\alpha_s)$ and $\mathcal{O}(\alpha^2)$, which represent the NLO QED corrections, where computed in Refs. [20,21].

The implementation of the full NLO QED corrections to the DGLAP evolution was achieved very recently in the APFEL program [11] following the approach of Ref. [14] and documented in Ref. [1]. A cross-check of the implementation was performed using the independent QEDEVOL code [12] based on the QCDNUM evolution program [13].

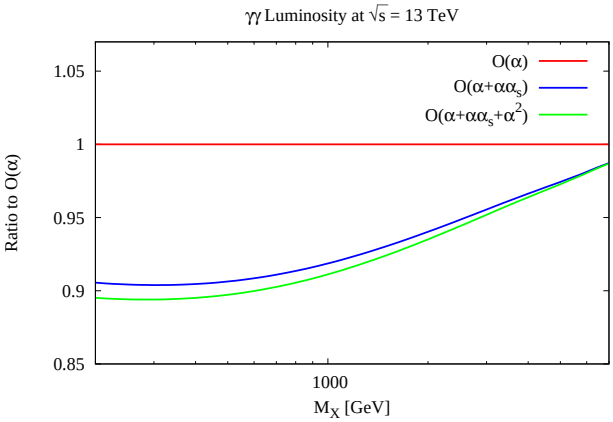

Fig. 3: $\gamma\gamma$ luminosity at $\sqrt{s} = 13$ TeV as a function of the final state invariant mass M_X obtained with NNPDF3.0QED NNLO. The curves, taking into account the $\mathcal{O}(\alpha)$, the $\mathcal{O}(\alpha+\alpha_s\alpha)$, and the complete $\mathcal{O}(\alpha+\alpha_s\alpha+\alpha^2)$ effects in the DGLAP evolution, are presented as ratios to the $\mathcal{O}(\alpha)$ result. set.

The effect of the NLO QED corrections on the $\gamma\gamma$ luminosity, relevant to the computation of the Drell-Yan invariant mass distribution, is shown in Fig. 3 as a function of the final state invariant mass M_X. The photon PDF taken from the NNPDF3.0QED set is evolved including in the DGLAP equation the $\mathcal{O}(\alpha)$, the $\mathcal{O}(\alpha+\alpha_s\alpha)$, and the complete $\mathcal{O}(\alpha+\alpha_s\alpha+\alpha^2)$ corrections. Results are shown as ratios to the $\mathcal{O}(\alpha)$ curve. While the effect of the $\mathcal{O}(\alpha^2)$ is very mild, the impact of the $\mathcal{O}(\alpha_s\alpha)$ at relatively small values of M_X can be as big as 10%. This reduces to around 3-5% at large invariant masses: this is the region of relevance in our study. This is still a significant effect due to the experimental uncertainty of the ATLAS data and thus it is important to take it into account.

In principle, the NLO QED corrections influence also the running of the QCD coupling α_s and the QED coupling α. In fact, they introduce additional mixing terms in the respective β-functions that couple the evolution of the two couplings. However, it turns out that the impact of the mixing terms is tiny on both couplings and thus we decided not to included them as this would uselessly complicated the implementation.

3.2 DIS structure functions

When considering NLO QED corrections to the DIS structure functions, it is necessary to include into the hard cross sections all the $\mathcal{O}(\alpha)$ diagrams. The coefficient functions of these diagrams, being of purely QED origin, can be easily derived from the QCD expressions by properly adjusting the colour factors. This correspondence holds irrespective of whether mass effects are included. This allowed for an easy implementation of the QED corrections to the FONLL general-mass scheme [22]. Specifically, in this work we have used the variant C of the FONLL scheme, accurate to NNLO in QCD, supplemented by the NLO QED corrections.

An intereresting feature of the NLO QED corrections to the DIS structure function is that they introduce photon-initiated diagrams providing a direct handle on the photon PDF. Fig. 4 displays the effect of the NLO QED corrections on the neutral-current structure functions F_2, F_L, and xF_3. The predictions have been obtained including the NLO QED corrections also to the DGLAP evolution and are shown normalised to the pure QCD results. The impact of the NLO QED corrections is very moderate especially at low x but becomes more significant at large x, where it is of the order of 2%. The same behaviour is observed also for the charged-current structure functions.

Although the net effect of the NLO QED corrections on the DIS structure functions is small, it is significant when compared to the typical size of the uncertainties of the HERA combined data. This implies that the DIS data, despite very moderately, contributes to constrain the photon PDF in the large-x region.

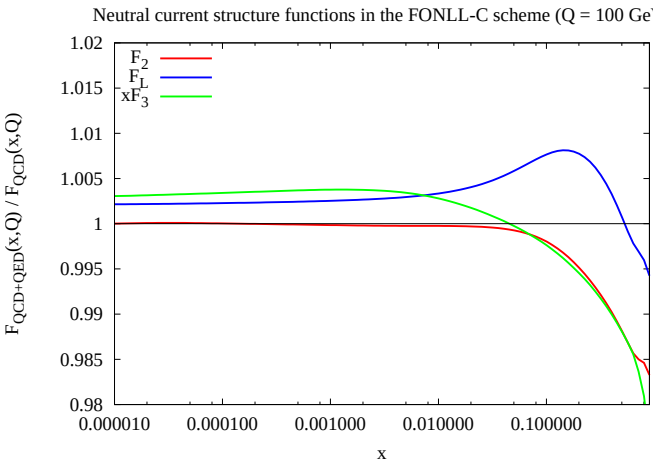

Fig. 4: Effects of the NLO QED corrections on the neutral-current DIS structure functions F_2, F_L and xF_3 at $Q = 100$ GeV as functions of x, normalised to the pure QCD results, obtained in the FONLL-C scheme using NNPDF3.0QED NNLO evolved including the QED corrections discussed above.

3.3 Drell-Yan cross sections

For the calculation of the Drell-Yan cross sections at NLO in QCD, we have used the `MadGraph5_aMC@NLO` [23] program interfaced to `APPLgrid` [24] through `aMCfast` [25]. The computation also includes the contribution from the photon-initiated diagrams shown in Fig. 1. Finite mass effects of charm and bottom quarks in the matrix elements are neglected, as appropriate for a high-scale process.

The NLO calculations are supplemented by K-factors obtained with the `FEWZ` code [26] to account for the NNLO QCD and the NLO EW corrections. The K-factors are defined as:

$$K(m_{ll}, |y_{ll}|) \equiv \frac{\text{NNLO QCD} + \text{NLO EW}}{\text{NLO QCD} + \text{LO EW}} \,, \tag{1}$$

and computed using the MMHT2014 NNLO [27] PDF set both in the numerator and in the denominator.

Fig. 5 shows the K-factors of Eq. (1) as a function of the lepton-pair rapidity $|y_{ll}|$ for each m_{ll} bin. The points correspond to the kinematics of double-differential distributions in $(m_{ll}, |y_{ll}|)$ of the ATLAS high-mass Drell-Yan data included in our analysis.

The K-factors vary between 0.98 and 1.04, indicating that higher-order corrections are generally moderate. The trend follows the expectation: the K-factors are particularly small at low invariant masses and in the central region, and tend to grow at larger values of m_{ll} and in the forward region where they can be as large ar 4%.

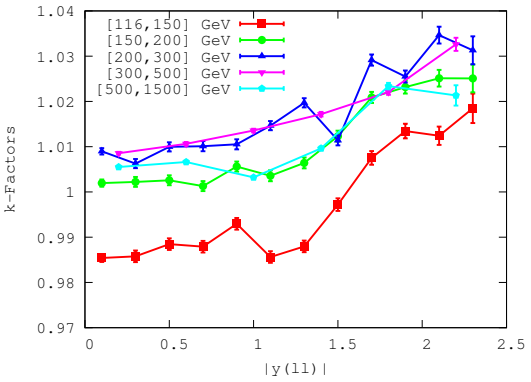

Fig. 5: The K-factors, defined in Eq. (1), as a function of the lepton-pair rapidity $|y_{ll}|$ for each m_{ll} bin.

4 Fit settings

Our determination of the photon PDF, along with quark and gluon PDFs, was carried out in the `xFitter` framework interfaced to the `APFEL` code. The dataset included in our fit was discussed in Sect. 2 and the theory setup presented in Sect. 3. In this section we discuss the fit settings.

We parametrise the following six independent distributions at the initial scale Q_0:

$$\begin{aligned}
xu(x,Q_0) - x\overline{u}(x,Q_0) \equiv xu_v(x,Q_0) &= A_{u_v} x^{B_{u_v}} (1-x)^{C_{u_v}} (1 + E_{u_v} x^2)\,, \\
xd(x,Q_0) - x\overline{d}(x,Q_0) \equiv xd_v(x,Q_0) &= A_{d_v} x^{B_{d_v}} (1-x)^{C_{d_v}}\,, \\
x\overline{u}(x,Q_0) \equiv x\bar{U}(x,Q_0) &= A_{\bar{U}} x^{B_{\bar{U}}} (1-x)^{C_{\bar{U}}}\,, \\
x\overline{d}(x,Q_0) + x\overline{s}(x,Q_0) \equiv x\bar{D}(x,Q_0) &= A_{\bar{D}} x^{B_{\bar{D}}} (1-x)^{C_{\bar{D}}}\,, \\
xg(x,Q_0) &= A_g x^{B_g} (1-x)^{C_g} (1 + E_g x^2)\,, \\
x\gamma(x,Q_0) &= A_\gamma x^{B_\gamma} (1-x)^{C_\gamma} (1 + D_\gamma x + E_\gamma x^2)\,.
\end{aligned} \tag{2}$$

The parameters $B_{\bar{U}}$ and $B_{\bar{D}}$ are set equal so that the quark sea distributions have the same small-x behaviour. Moreover, we assume $x\bar{s} = r_s x\bar{d}$, with $r_s = 1$ [28], and $A_{\bar{U}} = A_{\bar{D}}/2$, such that $x\bar{u} \to x\bar{d}$ for $x \to 0$.

The numerical values of the heavy-quark masses are taken to be $m_c = 1.47$ GeV and $m_b = 4.5$ GeV. The reference values of the QCD and QED couplings are chosen to be $\alpha_s(M_Z) = 0.118$ and $\alpha(m_\tau = 1.777\text{ GeV}) = 1/133.4$. As for the initial scale, we choose $Q_0 > m_c = \sqrt{7.5}$ GeV such that it is below the scale of all data points included in our fit. This particular value of the initial scale Q_0 is peculiar as compared to the typical choice $Q_0 < m_c \simeq 1$ GeV. The reason for choosing a somewhat larger scale is that it helps stabilise the photon PDF. However, in order to still be able to generate the charm PDFs perturbatively without the need to parameterise them, we exploited one of the functionalities of `APFEL` to set charm threshold $\mu_c = Q_0 > m_c$ [29].

5 Results

I finally turn to discuss the results of our fit. The partial χ^2's normalised to the number of data points for the HERA combined data and for the ATLAS high-mass Drell-yan data (bin by bin in m_{ll} and total), as well as the total χ^2 normalised to the number of degrees of freedom, are reported in Tab. 1. The overall fit quality is acceptably good. On the one hand, the description of the HERA data is comparable to that achieved in the HERAPDF2.0 analysis [16]. On the other hand, despite the small experimental uncertainties, the ATLAS Drell-Yan data is perfectly fitted with a $\chi^2/N_{\rm dat}$ equal to $48/48$. Remarkably, the single m_{ll} bins of this dataset have all a good χ^2.

Dataset	$\chi^2/N_{\rm dat}$
HERA combined DIS data	1236/1056
ATLAS DY data [116 GeV $\leq m_{ll} \leq$ 150 GeV]	9/12
ATLAS DY data [150 GeV $\leq m_{ll} \leq$ 200 GeV]	15/12
ATLAS DY data [200 GeV $\leq m_{ll} \leq$ 300 GeV]	14/12
ATLAS DY data [300 GeV $\leq m_{ll} \leq$ 500 GeV]	5/6
ATLAS DY data [500 GeV $\leq m_{ll} \leq$ 1500 GeV]	4/6
Total ATLAS DY data $\chi^2/N_{\rm dat}$	48/48
Combined HERA I+II and high-mass DY $\chi^2/N_{\rm dof}$	1284/1083

Table 1: $\chi^2/N_{\rm dat}$ of the fit to the combined HERA data and the five m_{ll} bins of the ATLAS Drell-Yan data. The global $\chi^2/N_{\rm dof}$ is also reported, where $N_{\rm dof}$ is the number of degrees of freedom in the fit.

The photon PDF at $Q^2 = 10^4$ GeV^2 obtained from our analysis, that we dubbed `xFitter_epHMDY`, is shown in Fig. 6 and compared to the LUXqed [7], the HKR16 [8], and the NNPDF3.0QED [5] results. The absolute distributions are shown in the lef plot, while they are displayed as ratios to the central value of `xFitter_epHMDY` in the right plot. The uncertainty bands represent the 68% confidence level for all distributions but for HKR16 for which only the central value is made available by the authors. The x-range shown Fig. 6 is limited to the region $0.02 \leq x \leq 0.9$ where the ATLAS Drell-Yan data are expected to constrain the photon PDF.

Fig. 6 shows that for $x \geq 0.1$ the four determinations are consistent within PDF uncertainties. For smaller values of x, the photon PDFs from LUXqed and HKR16 are lower than `xFitter_epHMDY` but the agreement remains at the 2-σ level. A better agreement with the NNPDF3.0QED photon PDF is observed all over the considered range also due to the larger uncertainties. Interestingly, Fig. 6 also shows that for $0.04 \leq x \leq 0.2$ the present analysis exhibits smaller PDF uncertainties as compared to those of NNPDF3.0QED. We conclude that this is the effect of the constraining power of the ATLAS

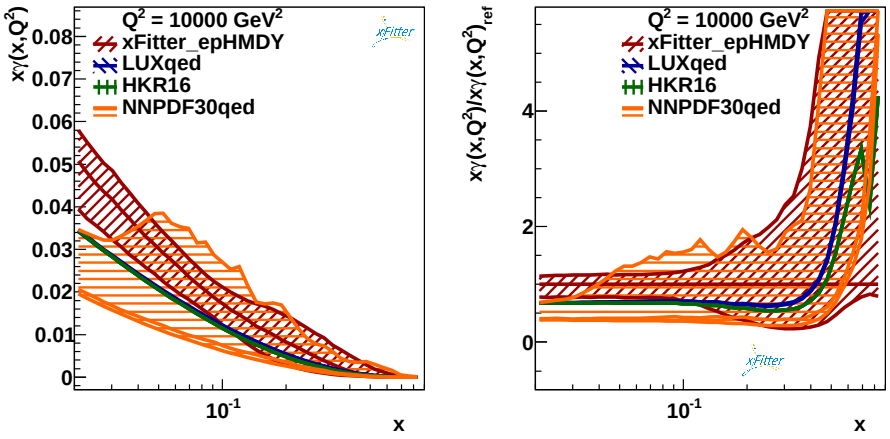

Fig. 6: Left plot: comparison between the photon PDF at $Q^2 = 10^4$ GeV^2 from the present analysis (`xFitter_epHMDY`) and the results from LUXqed, HKR16, and NNPDF3.0QED. Right plot: same as the left plot but with the distributions normalised to the central value of `xFitter_epHMDY`. The uncertainty bands represent the 68% confidence level. For HKR16 only the central value is available.

Drell-Yan data used in this analysis but not in NNPDF3.0QED. We also observe that this dataset has very little impact of the other PDFs.

Finally, in order to assess the robustness of our fit, we have performed a number of variations with respect to the default settings. Specifically, we considered variations of: the values of the input physical parameters, such as α_s, the heavy-quark masses m_c and m_b, and the strangeness fraction r_r; the PDF parametrisation and the input scale Q_0; the cut $Q^2_{\rm min}$ on the scale of the data included in the fit. In all cases, the resulting distributions of a given variation were in agreement, typically well within one standard deviation, with the result obtained with the default settings.

The `xFitter_epHMDY` presented in this work is available in the `LHAPDF6` format [30] upon request from the authors.

Acknowledgements

I would like to heartily thank Ringaile Plačakytė and Voica Radescu for their invaluable contribution to this work and for their outstanding dedication as conveners of the `HERAFitter-xFitter` project from 2012 until May 2017.

References

[1] F. Giuli *et al.* [xFitter Developers' Team], Eur. Phys. J. C **77** (2017) 400 doi:10.1140/epjc/s10052-017-4931-5 [arXiv:1701.08553 [hep-ph]].

[2] A. D. Martin, R. G. Roberts, W. J. Stirling and R. S. Thorne, Eur. Phys. J. C **39** (2005) 155 doi:10.1140/epjc/s2004-02088-7 [hep-ph/0411040].

[3] R. D. Ball *et al.* [NNPDF Collaboration], Nucl. Phys. B **877** (2013) 290 doi:10.1016/j.nuclphysb.2013.10.010 [arXiv:1308.0598 [hep-ph]].

[4] C. Schmidt, J. Pumplin, D. Stump and C. P. Yuan, Phys. Rev. D **93** (2016) 114015 doi:10.1103/PhysRevD.93.114015 [arXiv:1509.02905 [hep-ph]].

[5] V. Bertone and S. Carrazza, PoS DIS **2016** (2016) 031 [arXiv:1606.07130 [hep-ph]].

[6] R. D. Ball *et al.* [NNPDF Collaboration], JHEP **1504** (2015) 040 doi:10.1007/JHEP04(2015)040 [arXiv:1410.8849 [hep-ph]].

[7] A. Manohar, P. Nason, G. P. Salam and G. Zanderighi, Phys. Rev. Lett. **117** (2016) 242002 doi:10.1103/PhysRevLett.117.242002 [arXiv:1607.04266 [hep-ph]].

[8] L. A. Harland-Lang, V. A. Khoze and M. G. Ryskin, Phys. Rev. D **94** (2016) 074008 doi:10.1103/PhysRevD.94.074008 [arXiv:1607.04635 [hep-ph]].

[9] G. Aad *et al.* [ATLAS Collaboration], JHEP **1608** (2016) 009 doi:10.1007/JHEP08(2016)009 [arXiv:1606.01736 [hep-ex]].

[10] S. Alekhin *et al.*, Eur. Phys. J. C **75** (2015) 304 doi:10.1140/epjc/s10052-015-3480-z [arXiv:1410.4412 [hep-ph]].

[11] V. Bertone, S. Carrazza and J. Rojo, Comput. Phys. Commun. **185** (2014) 1647 doi:10.1016/j.cpc.2014.03.007 [arXiv:1310.1394 [hep-ph]].

[12] R. Sadykov, arXiv:1401.1133 [hep-ph].

[13] M. Botje, Comput. Phys. Commun. **182** (2011) 490 doi:10.1016/j.cpc.2010.10.020 [arXiv:1005.1481 [hep-ph]].

[14] V. Bertone, S. Carrazza, D. Pagani and M. Zaro, JHEP **1511** (2015) 194 doi:10.1007/JHEP11(2015)194 [arXiv:1508.07002 [hep-ph]].

[15] R. Boughezal, Y. Li and F. Petriello, Phys. Rev. D **89** (2014) 034030 doi:10.1103/PhysRevD.89.034030 [arXiv:1312.3972 [hep-ph]].

[16] H. Abramowicz *et al.* [H1 and ZEUS Collaborations], Eur. Phys. J. C **75** (2015) 580 doi:10.1140/epjc/s10052-015-3710-4 [arXiv:1506.06042 [hep-ex]].

[17] S. Moch, J. A. M. Vermaseren and A. Vogt, Nucl. Phys. B **688** (2004) 101 doi:10.1016/j.nuclphysb.2004.03.030 [hep-ph/0403192].

[18] A. Vogt, S. Moch and J. A. M. Vermaseren, Nucl. Phys. B **691** (2004) 129 doi:10.1016/j.nuclphysb.2004.04.024 [hep-ph/0404111].

[19] A. D. Martin, R. G. Roberts, W. J. Stirling and R. S. Thorne, Eur. Phys. J. C **39** (2005) 155 doi:10.1140/epjc/s2004-02088-7 [hep-ph/0411040].

[20] D. de Florian, G. F. R. Sborlini and G. Rodrigo, Eur. Phys. J. C **76** (2016) 282 doi:10.1140/epjc/s10052-016-4131-8 [arXiv:1512.00612 [hep-ph]].

[21] D. de Florian, G. F. R. Sborlini and G. Rodrigo, JHEP **1610** (2016) 056 doi:10.1007/JHEP10(2016)056 [arXiv:1606.02887 [hep-ph]].

[22] S. Forte, E. Laenen, P. Nason and J. Rojo, Nucl. Phys. B **834** (2010) 116 doi:10.1016/j.nuclphysb.2010.03.014 [arXiv:1001.2312 [hep-ph]].

[23] J. Alwall *et al.*, JHEP **1407** (2014) 079 doi:10.1007/JHEP07(2014)079 [arXiv:1405.0301 [hep-ph]].

[24] T. Carli *et al.*, Eur. Phys. J. C **66** (2010) 503 doi:10.1140/epjc/s10052-010-1255-0 [arXiv:0911.2985 [hep-ph]].

[25] V. Bertone, R. Frederix, S. Frixione, J. Rojo and M. Sutton, JHEP **1408** (2014) 166 doi:10.1007/JHEP08(2014)166 [arXiv:1406.7693 [hep-ph]].

[26] R. Gavin, Y. Li, F. Petriello and S. Quackenbush, Comput. Phys. Commun. **184** (2013) 208 doi:10.1016/j.cpc.2012.09.005 [arXiv:1201.5896 [hep-ph]].

[27] L. A. Harland-Lang, A. D. Martin, P. Motylinski and R. S. Thorne, Eur. Phys. J. C **75** (2015) 204 doi:10.1140/epjc/s10052-015-3397-6 [arXiv:1412.3989 [hep-ph]].

[28] M. Aaboud *et al.* [ATLAS Collaboration], Eur. Phys. J. C **77** (2017) 367 doi:10.1140/epjc/s10052-017-4911-9 [arXiv:1612.03016 [hep-ex]].

[29] V. Bertone *et al.* [xFitter Developers Team], arXiv:1707.05343 [hep-ph].

[30] A. Buckley *et al.*, Eur. Phys. J. C **75** (2015) 132 doi:10.1140/epjc/s10052-015-3318-8 [arXiv:1412.7420 [hep-ph]].